Hindawi
Journal of Nanomaterials
Volume 2018, Article ID 3091970, 10 pages
https://doi.org/10.1155/2018/3091970

Research Article

TiO_2-Intercalated Graphene Oxides with Highly Efficient Photocatalytic Degradation for Methylene Blue

Lirong Yao,[1] Li Dong,[1] Xiaojuan Li,[2] Sijun Xu,[1] Guangyu Zhang,[1] and Qilong Sun[1]

[1]*National & Local Joint Engineering Research Center of Technical Fiber Composites for Safety and Protection, Nantong University, Nantong 226019, China*
[2]*Faculty of Textile Science and Technology, Shinshu University, 3-15-1 Tokida, Ueda, Nagano 386-8567, Japan*

Correspondence should be addressed to Sijun Xu; xusijunwork@hotmail.com

Received 30 May 2018; Revised 23 September 2018; Accepted 30 September 2018; Published 19 December 2018

Academic Editor: Nageh K. Allam

The low photocatalytic decomposition activity of TiO_2 toward industrial pollutants at room temperature is one of the main obstacles for its practical application. TiO_2-intercalated graphene oxide (GO) composites were prepared by in situ hydrolysis of butyl titanate in a GO aqueous solution, followed by hydrothermal reaction to improve their photoelectron separation efficiency. The in situ generated TiO_2 nanocrystals could grow and adhere to the GO walls, thereby greatly improving the contact area and binding strength among them and resulting in low photoelectron transfer resistance. The photocatalytic activities of the as-prepared catalyst were evaluated via photodegradation of methylene blue (MB). The TiO_2-intercalated GOs displayed much higher catalytic activity than GO, TiO_2, and TiO_2-adsorbed GOs. The degradation efficiency of MB by TiO_2-intercalated GOs increased with increasing bath ratio of TiO_2-intercalated GOs to MB solution, but it decreased with increasing initial concentration of MB. Degradation of MB by UV light was much faster than by simulated sunlight. The degradation time by sunlight was only 5% of degradation time by UV light. Cyclic catalytic experiments indicated that TiO_2-intercalated GO maintained 99.97% degradation activity after repeated degradation (five times), thereby indicating the good decomposition durability.

1. Introduction

Solar energy has been used for 2.4 billion years. Plants, including algae, can generate carbohydrate using water, carbon dioxide, and sunlight. Photosynthesis has become a complex and efficient biochemical reaction that translates solar energy into organic matter. However, solar energy can also be transformed by many semiconductors, such as silicon, CdS, CdTe, GaAs, titanium oxide, zinc oxide, and perovskite. Among them, titanium oxide (TiO_2) is one of the most promising materials due to its advantages of low-cost, nontoxic, high physicochemical stability and transparency [1–5]. TiO_2 nanomaterials are widely used in organic wastewater treatment because of their excellent photocatalytic activity [6–17]. However, the high rate of electron-hole recombination is one of the main drawbacks of TiO_2 in photodegradation applications [18, 19].

To improve the photocatalytic efficiency, several methods, such as modification of TiO_2 nanoparticles with conductive organic materials, metal nanoparticles, and carbon materials, were developed to prevent electron-hole pair recombination [4, 20–24]. The integration of TiO_2 and graphene (GR) is intensively investigated, and advancement in this technology is obvious in recent studies because of the super photoelectric properties of GR. For example, TiO_2-GR nanocomposites have been prepared via a facile hydrothermal reaction of graphene oxide (GO) and TiO_2 in an ethanol-water solvent. Such TiO_2-GR nanocomposites exhibited much higher photocatalytic activity and stability toward benzene gas, which is a volatile aromatic pollutant in air, than bare TiO_2 [25]. Wen et al. prepared TiO_2-Ag-GR nanocomposites that showed significantly increased visible light absorption and photocatalytic activity compared with Ag-TiO_2 and TiO_2-GR nanocomposites [26]. Fan et al. compared TiO_2-reduced GO nanocomposites prepared by UV, hydrazine, and hydrothermal reductions. TiO_2-reduced GO composites prepared by the hydrothermal method exhibited optimal photocatalytic performance [27]. Nanakkal and Alexander developed

graphene/$BiVO_4$/TiO_2 ternary nanocomposites through a facile, ultrasonic wave-assisted one-pot hydrothermal method. The as-prepared composite exhibited enhanced photocatalytic degradation of methylene blue (MB) under visible light irradiation [28].

However, the photocatalytic efficiency of TiO_2-GR/TiO_2-GR is still limited because of the high contact resistance and low binding strength between prefabricated TiO_2 nanocrystals due to their large morphology mismatch and lack of chemical interactions that lead to low contact area [29]. To solve this problem, we synthesized closely integrated TiO_2-intercalated GO (TiO_2-GO-TiO_2 sandwich-like) composite nanosheets. TiO_2 could grow in situ on GOs and form the sandwich-like TiO_2-intercalated GO nanosheets by following hydrothermal reaction, when the hydrolysis and condensation of tetrabutyl titanate (TBOT) in GO solution is carefully controlled. The contact resistance and contact strength of TiO_2 nanocrystals can be greatly improved, because they grow by adhering to the GO surfaces [29]. The resultant TiO_2-intercalated GOs possessed a sandwich-like structure with an ultrathin nature and highly crystallized TiO_2 nanocrystals. Most importantly, the TiO_2-GO-TiO_2 nanosheets provide high photodecomposition efficiency and durability for the model dye, MB, compared with TiO_2 and TiO_2-adsorbed GOs [30–37].

2. Experimental

2.1. Materials and Reagents. The natural flake graphite (mesh = 1000) was purchased from Qingdao Jintao Graphite Co. Ltd. (China), and the TiO_2 was purchased from Jinan Jiyu Titanium Chemical Co. Ltd. (China). The concentrated sulfuric acid, potassium permanganate, hydrogen peroxide, hydrochloric acid, butyl titanate, and MB were purchased from Sinopharm Chemical Reagent Co. Ltd. (China) and were of analytical grade.

2.2. Synthesis of GOs, TiO_2-Intercalated GOs, and TiO_2-Adsorbed GOs. GOs were prepared from purified natural graphite by the modified Hummers method [38]. A total of 20 g of graphite and 460 mL of H_2SO_4 were mixed in a beaker container at 0°C under vigorous stirring. Then, 60 g of $KMnO_4$ was added to the suspension sample, maintaining a temperature of below 5°C. After addition of $KMnO_4$, the rising temperature should be maintained below 30°C for 30 min. The mixture was diluted with 1000 mL of DI water and heated to 95°C, maintaining this temperature for 15 min. Finally, 3000 mL of DI water and 100 mL of H_2O_2 were added to the mixture to terminate the reaction. The resultant mixture was washed with 10% of HCl aqueous solution, ultrasonicated for 30 min, and stored overnight. The suspension mixture was finally filtered, washed by DI water several times, and dried in a dry oven at 60°C.

The schematic of the preparation of TiO_2-intercalated GOs is presented in Figure 1. A 0.1 g of GOs was dissolved in 30 mL of DI water, sealed by a hydrothermal reactor (50 mL), and hydrothermally reacted at 135°C for 6 h. Then, the GO aqueous solution was ultrasonicated for 30 min, filtered, dried at 60°C, and then dissolved in tetrahydrofuran

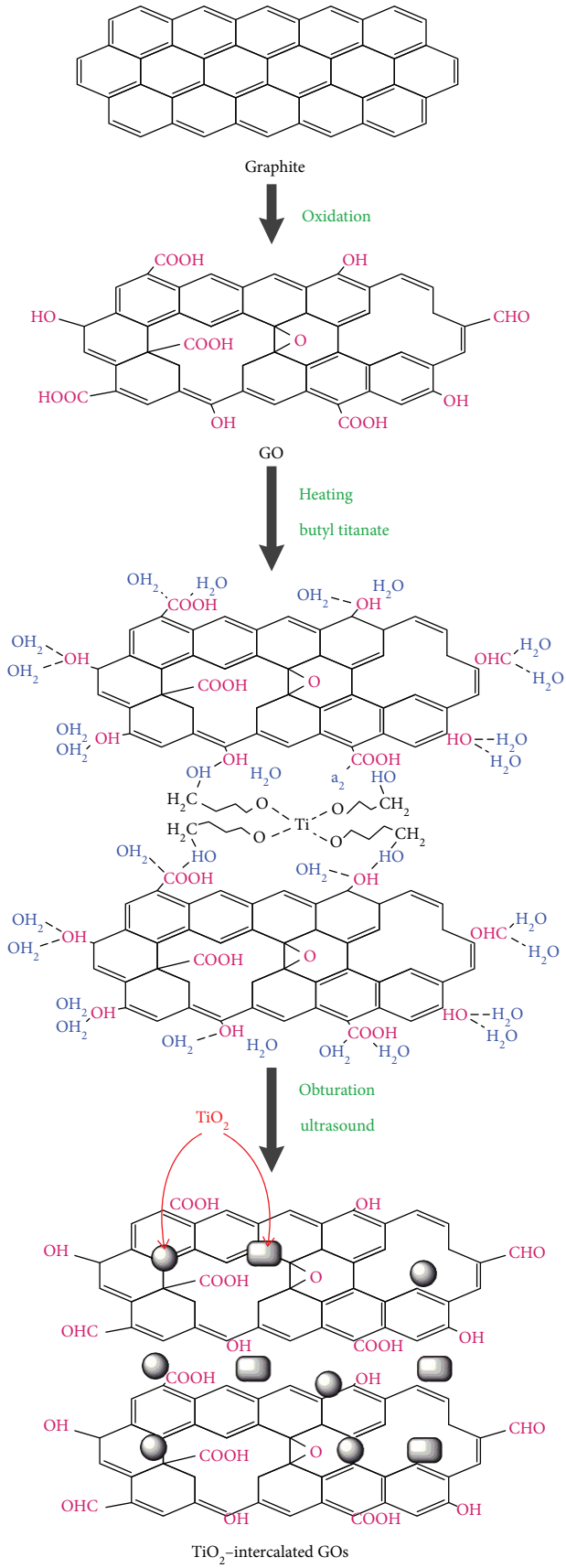

Figure 1: Scheme of the preparation of TiO_2-intercalated GOs.

with ultrasound treatment for three to four hours. Subsequently, 10–50 mL of butyl titanate was added into the GO solution and ultrasonicated for 30 min. The mixture was added into a hydrothermal reactor and crystallized at 180°C for 12 h. Finally, the resultant TiO_2-intercalated GO powder was filtered, washed, and finally dried at 60°C.

To synthesize TiO_2-adsorbed GOs (control), 40 mL of butyl titanate was added to 100 mL of absolute ethanol solution, after which 5 g of GOs was added. TiO_2-adsorbed GO solution was prepared by stirring for 5 h and then crystallized in a hydrothermal reactor at 180°C for 12 h. The obtained solution was centrifuged and dried at 60°C.

2.3. Characterizations. To identify the crystalline phase of synthesized samples, all samples were subjected to X-ray diffractometer (XRD; Shimata XD-D1, Japan) experiments at a scan speed of $2^\circ/m^{-1}$. The morphology of TiO_2 nanoparticles and GO sheets was observed by an S-3400N scanning electron microscope (SEM; Hitachi, Japan) and JEOL 2100F transmission electron microscope (TEM; JEOL, Japan) that operate at 200 kV accelerating voltage. The diffuse reflectance spectra were recorded on a TU-1901 ultraviolet-visible (UV-vis) spectrophotometer (PG Scientific, USA). Fourier transform infrared (FTIR) spectra were obtained on a Thermo Nicolet AVATAR 370 FTIR spectrometer (Bruker, Germany). The X-ray photoelectron spectra (XPS) were studied by the ESCALAB 250 XI X-ray photoelectron spectroscopy (Thermo Scientific, USA).

2.4. Photocatalytic Degradation of MB. The samples were added into 50 mL of the MB solutions and stored in the dark for 24 hours to reach the adsorption equilibrium. The obtained mixtures were placed onto a XPA-4 photochemical reactor (Xujiang Electromechanical Plant, China) with a 300 W UV light type mercury lamp and/or a 350 W solar-simulated xenon lamp. All light sources were located at 15 cm above the reaction solution. In the catalytic decomposition, 1 mL mixture was sampled and centrifuged at regular intervals. The supernatants were obtained and measured using a UV-vis spectrophotometer at a maximum absorption wavelength (λ max) of 664 nm to detect the MB concentration. To study the photocatalytic degradation of TiO_2-intercalated GOs toward MB in aqueous solution, we examined the initial MB concentration (ranging from 100–300 mg/L), the bath ratio between TiO_2-intercalated GOs and MB solution (1 : 50, 1 : 100, and 1 : 200), and the light source (without light, UV light, and simulated sunlight). The catalytic performances of the controls, TiO_2, GOs, and TiO_2-adsorbed GOs (prepared by adsorption of TiO_2 to GOs), were studied by following the experimental method.

The concentration C (mg/L) and the degradation rate D (%) were calculated according to the standard curve of MB. The calculation formula is as follows (1):

$$D = \frac{(C_0 - C_t)}{C_0} \times 100\%, \quad (1)$$

where C_0 is the initial concentration of MB, and C_t is the concentration of MB at time t.

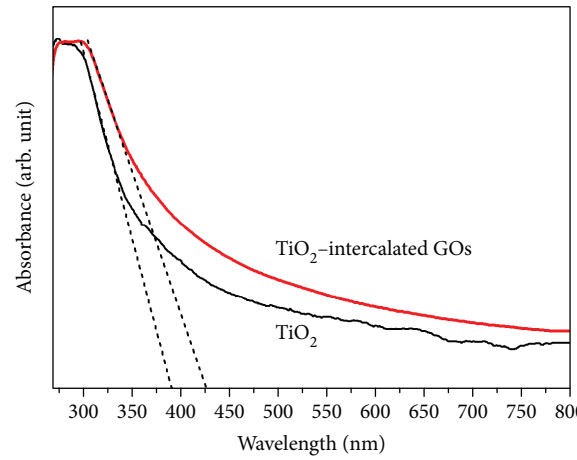

Figure 2: UV-vis spectra of TiO_2 and TiO_2-intercalated GOs.

3. Results and Discussion

The integration of TiO_2 and GOs may influence the adsorption band of TiO_2 because of the special electrochemical properties of GOs. The UV-vis absorption spectra in Figure 2 showed that the light absorption edge of TiO_2-intercalated GOs extended to about 426 nm while that of TiO_2 was only about 394 nm. The redshifts into the visible regions demonstrated the significant influence of GOs on the optical characteristics in which the adding of GOs narrowed the bandgap of TiO_2 owing to the formation of Ti–O–C chemical bonding in their interface [39, 40].

The FTIR spectra of graphite, GOs, and TiO_2-intercalated GOs are shown in Figure 3. The FTIR spectra of the natural flake graphite show a very smooth curve, indicating its poor infrared activity. A broad absorption band, which is a characteristic of the hydroxyl groups in GOs, can be observed at approximately 3430 cm^{-1}. In particular, 3500–3800 cm^{-1} exhibited a wide range of absorption peaks, which can be attributed to the absorbed water by GOs [41]. In addition, due to the hydroxyl groups in GOs, the FTIR spectra exhibited an absorption band in the vicinity of 1634 cm^{-1}, corresponding to the absorption peak for the bending vibration of O-H [42]. Furthermore, the band at the vicinity of 1720 cm^{-1} is attributed to the absorption of carboxylic acid and/or the carbonyl stretching vibration of C=O, which is attributed by –COOH and C=O in the surface and/or edge and of the GOs. The band observed at 1380 cm^{-1} is the stretching vibration of the epoxy groups (C-O-C) and carboxyl C-O in GOs [43]. The band in the vicinity of 1045 cm^{-1} is generated by the C-OH stretching vibration of GOs. All these absorption bands derived from the oxygen-containing groups in GO nanosheets. This indicates that graphite was fully oxidized and it generated abundant hydrophilic oxygen-containing groups. Hydrogen bonds were readily formed with water molecules because the GO surfaces contain these polar functional groups, thereby explaining the hydrophilic nature of GOs after the oxidation. For TiO_2-intercalated GOs, the absorption band near 3430 and 1634 cm^{-1}, representing the OH stretching and blending vibrations of GOs, respectively, weakened, whereas the C-O

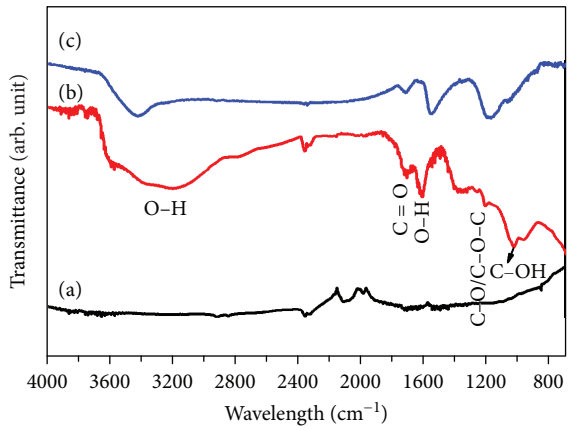

Figure 3: FTIR images of graphite, GOs, and TiO_2-intercalated GOs.

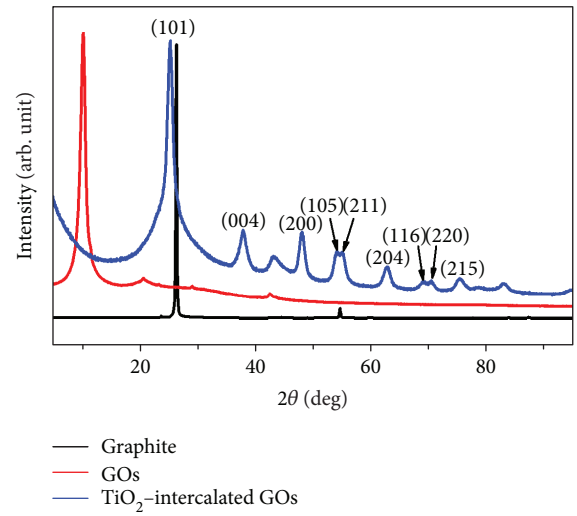

Figure 4: XRD patterns of graphite, GOs, and TiO_2-intercalated GOs.

adsorption at approximately 1045 cm^{-1} broadened. The OH groups in GOs were likely to form Ti-O-C during the hydrothermal reaction [29], suggesting the possible chemical interactions between TiO_2 and GOs.

The photocatalytic capability of TiO_2-intercalated GOs was derived from TiO_2 nanocrystals, which were mainly influenced by their crystal form, degree, and morphology. Figure 4 shows the XRD patterns of the natural flake graphite, GOs, and TiO_2-intercalated GOs. The characteristic diffraction peak was located at $2\theta = 30^\circ$ for the natural flake graphite. The XRD pattern of GO showed diffraction peaks at $2\theta = 10^\circ$, with lattice spacing of 0.887 nm. However, for TiO_2-intercalated GOs, several new peaks were detected at approximately $2\theta = 24.8^\circ$, $2\theta = 37.7^\circ$, $2\theta = 48.0^\circ$, $2\theta = 53.8^\circ$, $2\theta = 54.8^\circ$, $2\theta = 62.5^\circ$, $2\theta = 68.2^\circ$, $2\theta = 70.0^\circ$, and $2\theta = 74.8^\circ$, corresponding to the diffractions from the (101), (004), (200), (105), (211), (204), (116), (220), and (215) crystal planes of anatase TiO_2 (JCPDS card 21-1272), respectively [44]. In addition, the XRD signals of TiO_2 nanocrystals were extremely strong that the GO signals were completely concealed, thereby suggesting the high content of well-crystallized TiO_2 nanoparticles.

To examine the chemical composition and binding states of the samples, XPS spectra were collected, as displayed in Figure 5. All binding energies in the XPS experiments are trued by referring to the C1 (284.6 eV) peak. Figure 5(a) presents the wide-scan XPS spectra of GOs and TiO_2-intercalated GOs. TiO_2-intercalated GOs showed three strong peaks at 530.1, 454.8, and 284.1 eV, corresponding to O1s, Ti2p, and C1s [5, 45], respectively. However, only O1 and C1 signals were detected for GOs, indicating that Ti was successfully combined to GO surfaces. Figure 5(b) shows the C1 XPS spectra of TiO_2-intercalated GOs. The C1 XPS spectrum of TiO_2-intercalated GOs could be deconvoluted into three peaks, which were ascribed to sp^2 bonded carbon (C-C, 284.6 eV), epoxy/hydroxyls (C-O, 286.5 eV), and carboxyl (O=C-O, 288 eV) in line with GOs before the reaction [46, 47]. Therefore, GOs maintained their chemical construction after the hydrothermal reaction [48].

The distribution state of TiO_2 on/in the GO-GO surfaces and interlayers is significant for the catalytic activity of TiO_2 nanocrystals. The severe agglomeration of TiO_2 not only leads to low specific surface area but also to low contact efficiency of GO surfaces, thereby greatly influencing the electron-hole separation efficiency. The surface morphology and microscopic structure of the GOs and as-prepared TiO_2-intercalated GOs are initially observed by SEM (Figure 6). GOs were loosely stacked to form microsized layers (Figure 5(a)). Such loose structure was mainly caused by strong electrostatic repulsion among GOs due to the negatively charged oxygen-containing functional groups such as -OH and -COOH in GOs. After the reaction, as shown in Figure 5(b), the as-prepared TiO_2-intercalated GOs had abundant wrinkles and slight curling, indicating good flexibility. Most importantly, TiO_2 nanocrystals were almost uniformly monodispersed on the GO surfaces because these TiO_2 nanocrystals grow on OH, COOH-containing defect sites in the GO nanosheets, restricting their self-agglomeration. Such well-dispersed TiO_2 nanocrystals improved the photocatalytic efficiency of TiO_2-intercalated GO nanosheets by facilitating the generation and separation of electron-hole pairs.

The TiO_2 nanocrystals were not only attached to the GO surfaces but also to their interlamination. As shown in Figure 7(b), dense TiO_2 nanocrystals were found on and/or in the GOs, thereby suggesting that TiO_2 has good affinity to GOs [49]. To analyze the detailed hierarchical structure, the GO edge was observed in detail by HRTEM. As shown in Figure 6(a), two GO nanosheets were clearly observed. The nanosheets consisted of 8–10 one-atom thick GOs (arrows 1 and 2 in Figure 7(a)). Such multilayered GO nanosheets preserved certain conductivity and rigidity after oxidation. Notably, TiO_2 nanocrystals were found not only on the outer surface of GOs but also in the interlamination. As shown in box 1, these TiO_2 nanocrystals have relatively clear lattice fringes, indicating that they are on the upper surface of GOs. Interlaminar TiO_2 could be distinguished through careful confirmation of the relative space position between TiO_2

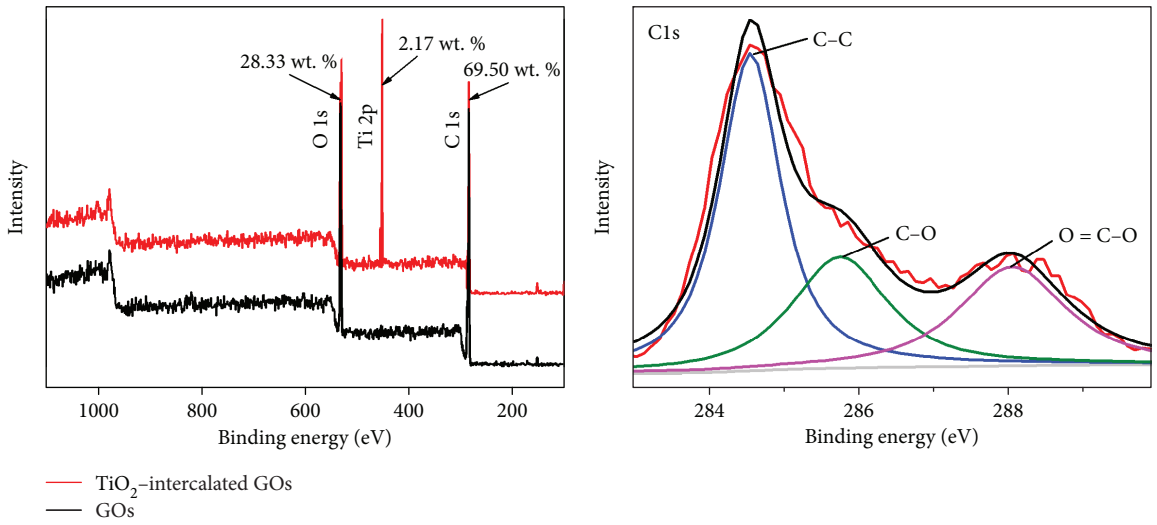

(a) (b)

Figure 5: (a) XPS spectra and (b) C1s XPS spectra of GOs and TiO_2-intercalated GOs.

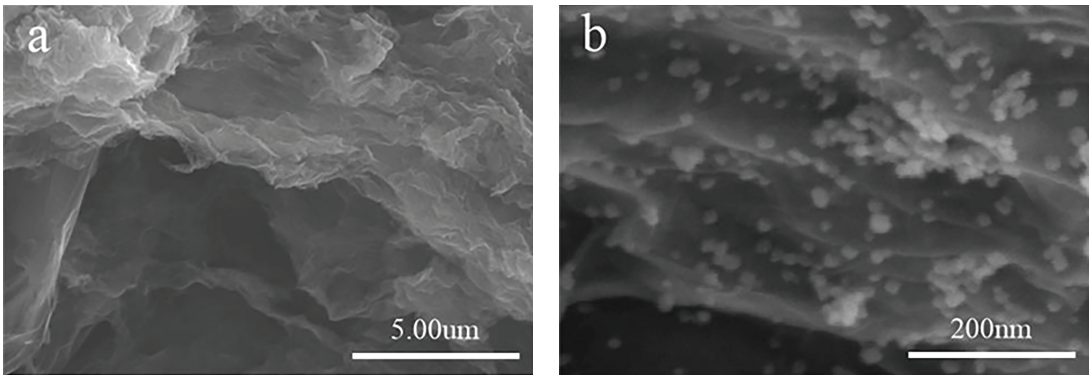

(a) (b)

Figure 6: SEM images of (a) GOs and (b) TiO_2-intercalated GOs.

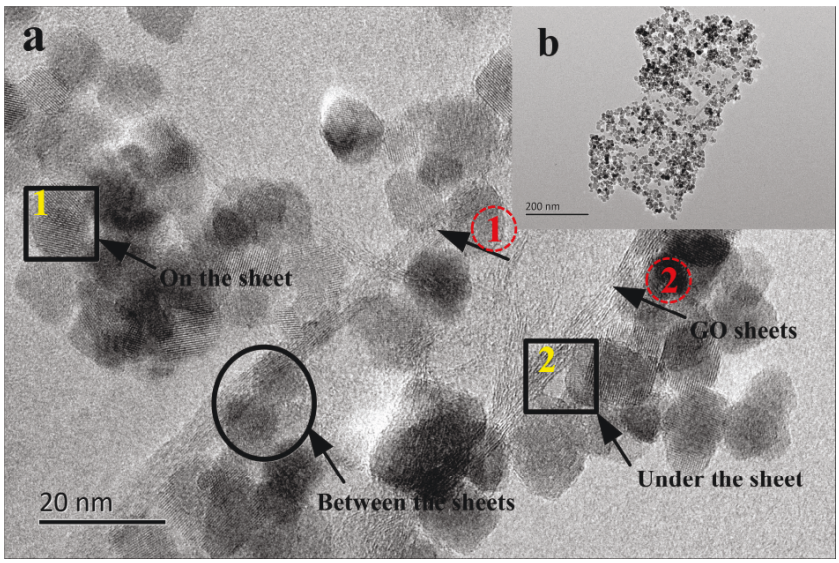

Figure 7: TEM images of TiO_2-intercalated GOs.

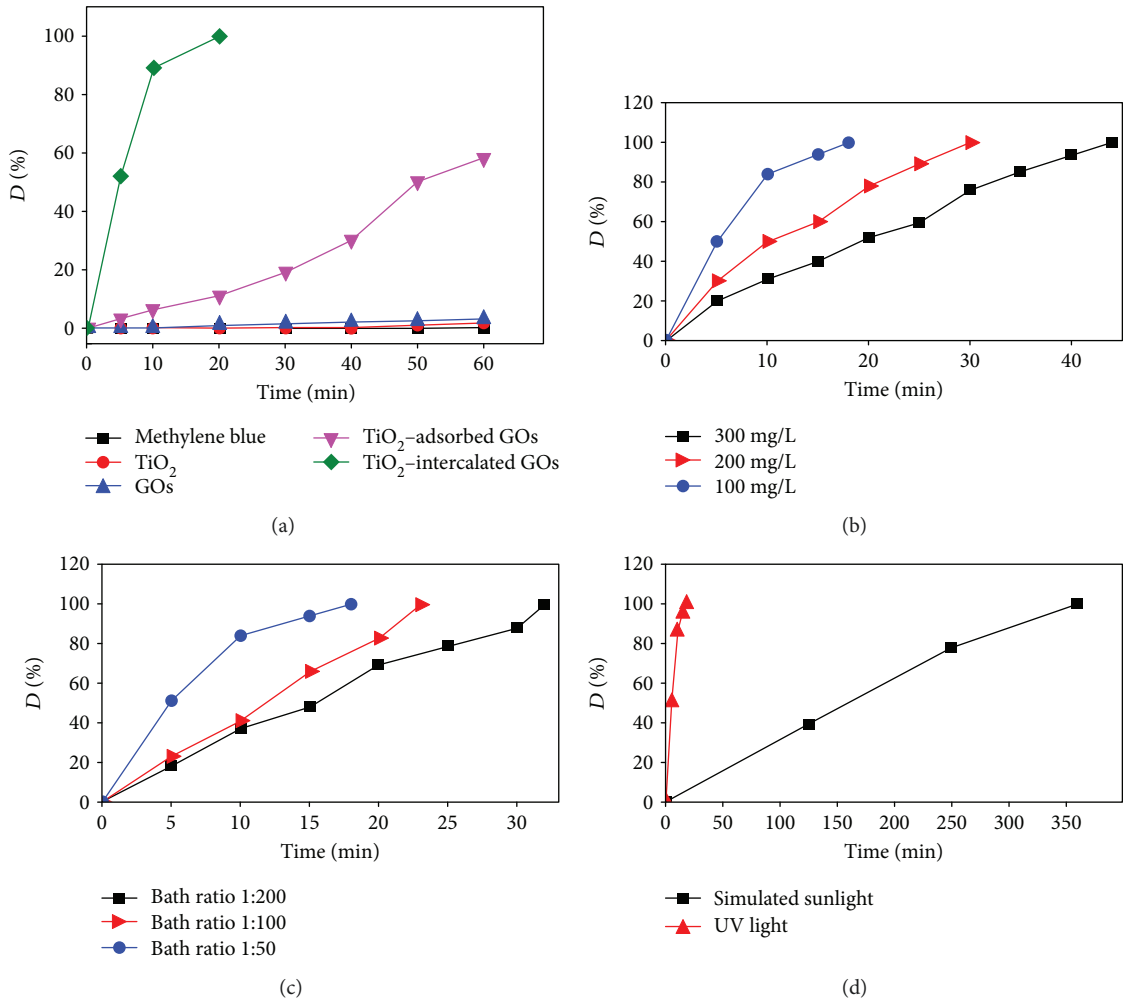

Figure 8: (a) Photocatalytic degradation of MB over TiO_2, GOs, TiO_2-adsorbed GOs, and TiO_2-intercalated GOs (experimental conditions: initial MB concentration of 100 mg/L, bath ratio of 1 : 50, and light source (UV light)). (b) Effect of MB concentration on the TiO_2-intercalated GO degradation of MB (experimental conditions: bath ratio (1 : 50) and light condition (UV light)). (c) Effect of bath ratio on the photodegradation rate of MB (experimental conditions: initial MB concentration (100 mg/L) and light condition (UV light)). (d) Effect of light conditions on the TiO_2-intercalated GO degradation of MB (experimental conditions: initial MB concentration (100 mg/L) and bath ratio (1 : 50)).

and GO nanosheets. As shown in the circle, TiO_2 nanocrystals were clamped by two GO nanosheets, evidencing the sandwich structure. Similarly, as shown in box 2, the TiO_2 nanocrystals covered by bottomed GOs proved that they are on the lower GO surfaces.

3.1. Photocatalytic Degradation of MB. The photocatalytic activities of TiO_2-intercalated GOs, TiO_2-adsorbed GOs, GOs, and TiO_2 for MB were evaluated. As shown in Figure 8(a), GOs and TiO_2 showed relatively weak photocatalytic activity toward MB. For TiO_2-adsorbed GOs, only ~60% of MB was decomposed after 1 h UV radiation. On the contrary, the TiO_2-intercalated GOs exhibited much higher photocatalytic degradation efficiency than other catalysts (TiO_2-intercalated GOs > TiO_2-adsorbed GOs > GOs > TiO_2). They could degrade nearly 99.9% of MB within 18 min under the UV light which was much faster than reported literature [25, 33, 50–53]. Because of in situ growth of TiO_2 nanocrystals by adhering to GO surfaces and/or GO-GO interfaces, the contact resistance between TiO_2 and GOs was significantly reduced. As a result, the photoelectron generated by TiO_2 could be efficiently led away by GOs, thereby greatly improving the separation of electron-hole pairs on TiO_2 surfaces. In addition, GO nanosheets could help TiO_2 to adsorb MB organic molecules due to their huge surface area and abundant anionic OH and COOH groups.

To study the effect of MB initial concentration on the photocatalytic degradation efficiency, the photocatalytic degradation experiments were conducted with MB concentrations that range from 100 mg/L to 300 mg/L, while maintaining other parameters constant. As shown in Figure 8(b), TiO_2-intercalated GOs nearly completely degraded MB when MB concentration even reached up to 300 mg/L, indicating their high catalytic capacity. The complete degradation time for 100–300 mg/L of MB was 18, 30, and 60 min, suggesting the high catalytic efficiency of TiO_2-intercalated GOs. The

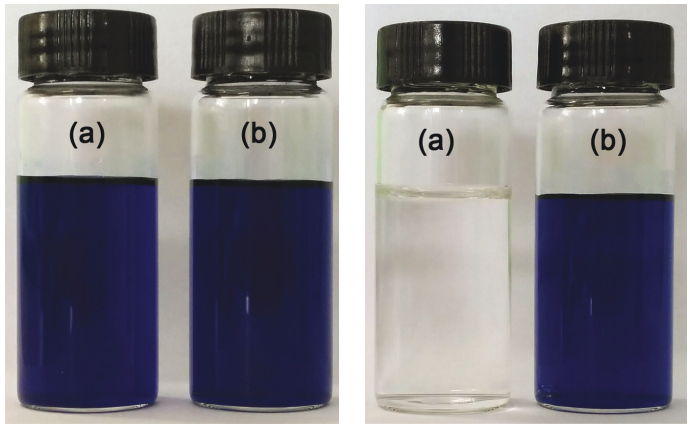

Figure 9: MB (a) with and (b) without UV radiation in the presence of TiO_2-intercalated GOs (experimental conditions: initial MB concentration of 100 mg/L, bath ratio of 1 : 50, and light source (UV light)).

calculated photodegradation efficiency of TiO_2-intercalated GOs showed significant decrease with increase in MB concentration because of the incident of UV light depth which became shallower with increasing MB concentration, thereby greatly reducing the photodegradation efficiency in the low solution.

To study the effect of the bath ratio between the TiO_2-intercalated GO catalyst and MB solution on the photocatalytic degradation performance, 0.5–2 g TiO_2-intercalated GOs was added into 100 g of 100 mg/L MB solution, while maintaining the other parameters constant. As presented in Figure 8(c), although the photodegradation ratio of MB changed with increasing bath ratio, the corresponding photodegradation rate of TiO_2-intercalated GOs toward MB increased. The nearly complete photodegradation time for MB stretched from 18 min to 23 min and then to 32 min. Thus, the increase in the mass of TiO_2-intercalated GOs could improve the photodegradation efficiency toward MB.

We varied the light conditions (simulated sunlight and UV light) to test their influence on the photocatalytic degradation of MB. As shown in Figure 8(d), 99.99% of MB was degraded by TiO_2-intercalated GOs for only 18 min under UV light, whereas only 99.89% degradation efficiency was obtained under 360 min sunlight irradiation. The degradation time under UV light is only 5% of that under simulated sunlight. The low degradation efficiency is caused by the UV light, which only accounts for a small fraction (3%–5%) of the sunlight, whereas the TiO_2-intercalated GOs only showed photocatalytic degradation activity in the UV band. However, the TiO_2-intercalated GOs could degrade 99.89% of MB under 360 min (<6 h) simulated sunlight irradiation, still indicating their good applicability.

Figure 9 showed MB with and without UV radiation in the presence of TiO_2-intercalated GOs. The color of MB with UV radiation soon became shallow and finally colorless, whereas that without UV radiation showed no obvious change after 20 min magnetic stirring in the dark. This indicates that physical adsorption by GOs was negligible during short UV irradiation probably because a number of OH and COOH groups reacted with TiO_2 to form Ti-O-C groups. The high treatment efficiency for MB should mainly attribute to the high photodegradation of TiO_2-intercalated GOs.

To further demonstrate the decomposition durability, the circulating runs of the TiO_2-intercalated GO catalyst in the photocatalytic degradation of MB were carried out. After the complete photodegradation of MB every time, TiO_2-intercalated GO catalyst was collected, washed, dried at 60°C, and used for the next photodegradation cycle. As shown in Figure 10, the TiO_2-intercalated GO catalyst did not exhibit evident significant loss of photocatalytic activity after four runs of MB degradation. The photodegradation rate of MB reached up to 99.98%, 99.98%, 99.99%, and 99.97% after two to four times of circulation. The relative degradation time was 24, 32, 41, and 70 min. Nevertheless, after five times of circulation photodegradation, the TiO_2-intercalated GOs obtained only 55.47% photodegradation rate even after 330 min UV light irradiation. The results indicated that the optimal cycle time of TiO_2-intercalated GOs was four times. To examine the possible damage for the chemical structure of TiO_2-intercalated GOs during prolonged exposure to UV light, FTIR spectra of TiO_2-intercalated GOs before and after six-cycle UV irradiation were measured (Figure 11). The adsorption intensity of OH groups for TiO_2-intercalated GOs slightly weakened after six time cycles while the chemical construction remained unchanged, indicating the high chemical stability. The decrease in hydroxyl, small molecular contamination, and interlayer blocking may be responsible for the weakened photocatalytic performance after five time cycles.

4. Conclusion

In summary, we demonstrate a synthesis strategy of sandwich-like TiO_2-intercalated GO nanosheets to improve the contact area between TiO_2 and GOs. Our FIIR, XPS, and XRD measurements showed that the as-prepared TiO_2-intercalated GOs maintained the inherent chemical construction of GOs and generated high content and high

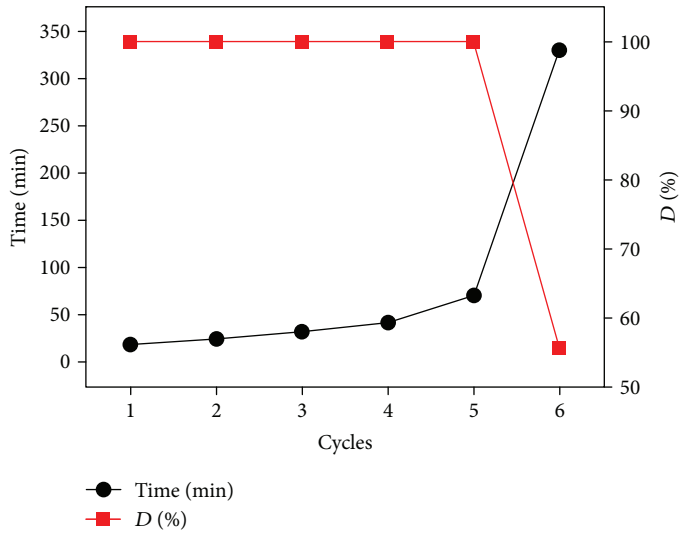

Figure 10: Decomposition durability of TiO_2-intercalated GOs (experimental conditions: initial MB concentration of 100 mg/L, bath ratio of 1 : 50, and light source (UV light)).

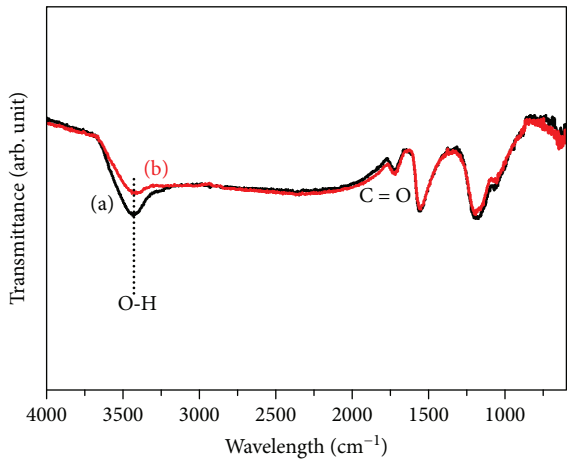

Figure 11: FTIR spectra of TiO_2-intercalated GOs with (a) zero and (b) six runs of MB degradation.

crystallized TiO_2 nanoparticles after the hydrothermal reaction. The SEM and TEM results indicated that TiO_2 nanocrystals were uniformly dispersed on and in GO nanosheets, forming an independent sandwich-like structure. Notably, GOs consisted of 8–10 layered one-atom thick GOs. Such structure was beneficial to maintain certain electric conductivity of GOs. In addition, the photocatalytic activities of the as-prepared catalyst were further studied using methylene blue as a degradation sample. The results indicated that the catalytic activity of the TiO_2-intercalated GOs was much stronger than pure TiO_2 and TiO_2-adsorbed GOs. Moreover, decreasing the initial concentration of MB and increasing the bath ratio of TiO_2-intercalated GOs could increase the degradation efficiency of MB. The contrast tests further indicated that the degradation of MB by UV light was much faster than that by simulated sunlight. The final cyclic photodegradation test showed that the TiO_2-intercalated GOs maintained 99.97% degradation activity after four times of repeated degradation, indicating good decomposition durability.

Data Availability

The data used to support the findings of this study are included within the article.

Conflicts of Interest

The authors declare that they have no competing interests.

Acknowledgments

The authors acknowledge the financial support of the National Natural Science Foundation of China (Young Foundation) (no. 51703098 and no. 51503105) and Jiangsu Qing Lan Project.

References

[1] M. Xing, J. Zhang, and F. Chen, "New approaches to prepare nitrogen-doped TiO_2 photocatalysts and study on their photocatalytic activities in visible light," *Applied Catalysis B: Environmental*, vol. 89, no. 3-4, pp. 563–569, 2009.

[2] X. Feng, K. Zhu, A. J. Frank, C. A. Grimes, and T. E. Mallouk, "Rapid charge transport in dye-sensitized solar cells made from vertically aligned single-crystal rutile TiO_2 nanowires," *Angewandte Chemie International Edition*, vol. 51, no. 11, pp. 2727–2730, 2012.

[3] Z. Bian, T. Tachikawa, and T. Majima, "Superstructure of TiO_2 crystalline nanoparticles yields effective conduction pathways for photogenerated charges," *The Journal of Physical Chemistry Letters*, vol. 3, no. 11, pp. 1422–1427, 2012.

[4] B. Qiu, M. Xing, and J. Zhang, "Mesoporous TiO_2 nanocrystals grown in situ on graphene aerogels for high photocatalysis and lithium-ion batteries," *Journal of the American Chemical Society*, vol. 136, no. 16, pp. 5852–5855, 2014.

[5] K. Zhang, J. K. Kim, B. Park et al., "Defect-induced epitaxial growth for efficient solar hydrogen production," *Nano Letters*, vol. 17, no. 11, pp. 6676–6683, 2017.

[6] T. Kuwabara, H. Sugiyama, M. Kuzuba, T. Yamaguchi, and K. Takahashi, "Inverted bulk-heterojunction organic solar cell using chemical bath deposited titanium oxide as electron collection layer," *Organic Electronics*, vol. 11, no. 6, pp. 1136–1140, 2010.

[7] A. Gholami, I. Khazaee, S. Eslami, M. Zandi, and E. Akrami, "Experimental investigation of dust deposition effects on photo-voltaic output performance," *Solar Energy*, vol. 159, pp. 346–352, 2018.

[8] X. Kong, C. Liu, W. Dong et al., "Metal-semiconductor-metal TiO_2 ultraviolet detectors with Ni electrodes," *Applied Physics Letters*, vol. 94, no. 12, article 123502, 2009.

[9] Y. Wang, H. Yu, C. Chen, and Z. Zhao, "Review of the biocompatibility of micro-arc oxidation coated titanium alloys," *Materials & Design*, vol. 85, pp. 640–652, 2015.

[10] K. R. Reddy, M. Hassan, and V. G. Gomes, "Hybrid nanostructures based on titanium dioxide for enhanced photocatalysis," *Applied Catalysis A: General*, vol. 489, pp. 1–16, 2015.

[11] T. Luttrell, S. Halpegamage, J. Tao, A. Kramer, E. Sutter, and M. Batzill, "Why is anatase a better photocatalyst than rutile? - Model studies on epitaxial TiO_2 films," *Scientific Reports*, vol. 4, no. 1, p. 4043, 2014.

[12] C. Cheng, A. Amini, C. Zhu, Z. Xu, H. Song, and N. Wang, "Enhanced photocatalytic performance of TiO_2-ZnO hybrid nanostructures," *Scientific Reports*, vol. 4, no. 1, p. 4181, 2014.

[13] N. Ahmed, A. A. Farghali, W. M. A. El Rouby, and N. K. Allam, "Enhanced photoelectrochemical water splitting characteristics of TiO_2 hollow porous spheres by embedding graphene as an electron transfer channel," *International Journal of Hydrogen Energy*, vol. 42, no. 49, pp. 29131–29139, 2017.

[14] W. A. Abbas, M. Ramadan, A. Y. Faid et al., "Photoactive catalysts for effective water microbial purification: morphology-activity relationship," *Environmental Nanotechnology, Monitoring & Management*, vol. 10, pp. 87–93, 2018.

[15] M. Ramadan, H. M. A. Hassan, A. Shahat, R. F. M. Elshaarawy, and N. K. Allam, "Ultrahigh performance of novel energy-efficient capacitive deionization electrodes based on 3D nanotubular composites," *New Journal of Chemistry*, vol. 42, no. 5, pp. 3560–3567, 2018.

[16] M. Ramadan, A. M. Abdellah, S. G. Mohamed, and N. K. Allam, "3D interconnected binder-free electrospun MnO@C nanofibers for supercapacitor devices," *Scientific Reports*, vol. 8, no. 1, p. 7988, 2018.

[17] A. S. Hassanien, R. A. Shedeed, and N. K. Allam, "Graphene quantum sheets with multiband emission: unravelling the molecular origin of graphene quantum dots," *The Journal of Physical Chemistry C*, vol. 120, no. 38, pp. 21678–21684, 2016.

[18] S. G. Kumar and L. G. Devi, "Review on modified TiO_2 photocatalysis under UV/visible light: selected results and related mechanisms on interfacial charge carrier transfer dynamics," *The Journal of Physical Chemistry A*, vol. 115, no. 46, pp. 13211–13241, 2011.

[19] G. Mele, C. Annese, L. D'Accolti et al., "Photoreduction of carbon dioxide to formic acid in aqueous suspension: a comparison between phthalocyanine/TiO_2 and porphyrin/TiO_2 catalysed processes," *Molecules*, vol. 20, no. 1, pp. 396–415, 2015.

[20] T. Morikawa, R. Asahi, T. Ohwaki, K. Aoki, and Y. Taga, "Band-gap narrowing of titanium dioxide by nitrogen doping," *Japanese Journal of Applied Physics*, vol. 40, 6A, Part 2, pp. L561–L563, 2001.

[21] C. Belver, C. Han, J. J. Rodriguez, and D. D. Dionysiou, "Innovative W-doped titanium dioxide anchored on clay for photocatalytic removal of atrazine," *Catalysis Today*, vol. 280, pp. 21–28, 2017.

[22] Y. Zhang, Y. Meng, K. Zhu et al., "Copper-doped titanium dioxide bronze nanowires with superior high rate capability for lithium ion batteries," *ACS Applied Materials & Interfaces*, vol. 8, no. 12, pp. 7957–7965, 2016.

[23] S. Na Phattalung, S. Limpijumnong, and J. Yu, "Passivated co-doping approach to bandgap narrowing of titanium dioxide with enhanced photocatalytic activity," *Applied Catalysis B: Environmental*, vol. 200, pp. 1–9, 2017.

[24] Q. Xiang, J. Yu, and M. Jaroniec, "Graphene-based semiconductor photocatalysts," *Chemical Society Reviews*, vol. 41, no. 2, pp. 782–796, 2012.

[25] Y. Zhang, Z. R. Tang, X. Fu, and Y. J. Xu, "TiO_2–graphene nanocomposites for gas-phase photocatalytic degradation of volatile aromatic pollutant: is TiO_2–graphene truly different from other TiO_2–carbon composite materials?," *ACS Nano*, vol. 4, no. 12, pp. 7303–7314, 2010.

[26] Y. Wen, H. Ding, and Y. Shan, "Preparation and visible light photocatalytic activity of Ag/TiO_2/graphene nanocomposite," *Nanoscale*, vol. 3, no. 10, pp. 4411–4417, 2011.

[27] W. Fan, Q. Lai, Q. Zhang, and Y. Wang, "Nanocomposites of TiO_2 and reduced graphene oxide as efficient photocatalysts for hydrogen evolution," *The Journal of Physical Chemistry C*, vol. 115, no. 21, pp. 10694–10701, 2011.

[28] A. R. Nanakkal and L. K. Alexander, "Graphene/$BiVO_4$/TiO_2 nanocomposite: tuning band gap energies for superior photocatalytic activity under visible light," *Journal of Materials Science*, vol. 52, no. 13, pp. 7997–8006, 2017.

[29] W. Li, F. Wang, Y. Liu et al., "General strategy to synthesize uniform mesoporous TiO_2/graphene/mesoporous TiO_2 sandwich-like nanosheets for highly reversible lithium storage," *Nano Letters*, vol. 15, no. 3, pp. 2186–2193, 2015.

[30] Y. Cong, M. Long, Z. Cui et al., "Anchoring a uniform TiO_2 layer on graphene oxide sheets as an efficient visible light photocatalyst," *Applied Surface Science*, vol. 282, pp. 400–407, 2013.

[31] D. Zhao, G. Sheng, C. Chen, and X. Wang, "Enhanced photocatalytic degradation of methylene blue under visible irradiation on graphene@TiO_2 dyade structure," *Applied Catalysis B: Environmental*, vol. 111-112, pp. 303–308, 2012.

[32] H. Sun, S. Liu, S. Liu, and S. Wang, "A comparative study of reduced graphene oxide modified TiO_2, ZnO and Ta_2O_5 in visible light photocatalytic/photochemical oxidation of methylene blue," *Applied Catalysis B: Environmental*, vol. 146, pp. 162–168, 2014.

[33] N. Raghavan, S. Thangavel, and G. Venugopal, "Enhanced photocatalytic degradation of methylene blue by reduced graphene-oxide/titanium dioxide/zinc oxide ternary nanocomposites," *Materials Science in Semiconductor Processing*, vol. 30, pp. 321–329, 2015.

[34] X. Luan, M. T. Gutierrez Wing, and Y. Wang, "Enhanced photocatalytic activity of graphene oxide/titania nanosheets composites for methylene blue degradation," *Materials Science in Semiconductor Processing*, vol. 30, pp. 592–598, 2015.

[35] Y. Min, K. Zhang, W. Zhao, F. Zheng, Y. Chen, and Y. Zhang, "Enhanced chemical interaction between TiO_2 and graphene oxide for photocatalytic decolorization of methylene blue," *Chemical Engineering Journal*, vol. 193-194, pp. 203–210, 2012.

[36] S. Liu, H. Sun, S. Liu, and S. Wang, "Graphene facilitated visible light photodegradation of methylene blue over titanium dioxide photocatalysts," *Chemical Engineering Journal*, vol. 214, pp. 298–303, 2013.

[37] X. Shao, W. Lu, R. Zhang, and F. Pan, "Enhanced photocatalytic activity of TiO_2-C hybrid aerogels for methylene blue degradation," *Scientific Reports*, vol. 3, no. 1, p. 3018, 2013.

[38] W. S. Hummers Jr. and R. E. Offeman, "Preparation of graphitic oxide," *Journal of the American Chemical Society*, vol. 80, no. 6, pp. 1339–1339, 1958.

[39] K. Zhang, L. Wang, J. K. Kim et al., "An order/disorder/water junction system for highly efficient co-catalyst-free photocatalytic hydrogen generation," *Energy & Environmental Science*, vol. 9, no. 2, pp. 499–503, 2016.

[40] K. Zhang, K. C. Kemp, and V. Chandra, "Homogeneous anchoring of TiO_2 nanoparticles on graphene sheets for waste water treatment," *Materials Letters*, vol. 81, pp. 127–130, 2012.

[41] W.-D. Yang, Y.-R. Li, and Y.-C. Lee, "Synthesis of r-GO/TiO_2 composites via the UV-assisted photocatalytic reduction of graphene oxide," *Applied Surface Science*, vol. 380, pp. 249–256, 2016.

[42] J. Liu, H. Bai, Y. Wang, Z. Liu, X. Zhang, and D. D. Sun, "Self-assembling TiO_2 nanorods on large graphene oxide sheets at a two-phase interface and their anti-recombination in photocatalytic applications," *Advanced Functional Materials*, vol. 20, no. 23, pp. 4175–4181, 2010.

[43] A. Bagri, C. Mattevi, M. Acik, Y. J. Chabal, M. Chhowalla, and V. B. Shenoy, "Structural evolution during the reduction of chemically derived graphene oxide," *Nature Chemistry*, vol. 2, no. 7, pp. 581–587, 2010.

[44] Y. F. You, C. H. Xu, S. S. Xu et al., "Structural characterization and optical property of TiO_2 powders prepared by the sol–gel method," *Ceramics International*, vol. 40, no. 6, pp. 8659–8666, 2014.

[45] K. Baba and R. Hatada, "Synthesis and properties of TiO_2 thin films by plasma source ion implantation," *Surface and Coatings Technology*, vol. 136, no. 1-3, pp. 241–243, 2001.

[46] J. Oh, S. Lee, K. Zhang et al., "Graphene oxide-assisted production of carbon nitrides using a solution process and their photocatalytic activity," *Carbon*, vol. 66, pp. 119–125, 2014.

[47] K. Zhang, N. Heo, X. Shi, and J. H. Park, "Chemically modified graphene oxide-wrapped quasi-micro Ag decorated silver trimolybdate nanowires for photocatalytic applications," *The Journal of Physical Chemistry C*, vol. 117, no. 45, pp. 24023–24032, 2013.

[48] Y.-H. Lin, H.-D. Lin, C.-K. Liu et al., "Annealing effect on the structural, mechanical and electrical properties of titanium-doped diamond-like carbon films," *Thin Solid Films*, vol. 518, no. 5, pp. 1503–1507, 2009.

[49] Z. D. Meng and W. C. Oh, "Sonocatalytic degradation and catalytic activities for MB solution of Fe treated fullerene/TiO_2 composite with different ultrasonic intensity," *Ultrasonics Sonochemistry*, vol. 18, no. 3, pp. 757–764, 2011.

[50] B.-K. Choi, W.-K. Choi, S.-J. Park, and M.-K. Seo, "One-pot synthesis of Ag-TiO_2/nitrogen-doped graphene oxide nanocomposites and its photocatalytic degradation of methylene blue," *Journal of Nanoscience and Nanotechnology*, vol. 18, no. 9, pp. 6075–6080, 2018.

[51] Y. Yang, L. Xu, H. Wang, W. Wang, and L. Zhang, "TiO_2/graphene porous composite and its photocatalytic degradation of methylene blue," *Materials & Design*, vol. 108, pp. 632–639, 2016.

[52] H. Safardoust-Hojaghan and M. Salavati-Niasari, "Degradation of methylene blue as a pollutant with N-doped graphene quantum dot/titanium dioxide nanocomposite," *Journal of Cleaner Production*, vol. 148, pp. 31–36, 2017.

[53] Y. Liu, Y. Shi, X. Liu, and H. Li, "A facile solvothermal approach of novel Bi_2S_3/TiO_2/RGO composites with excellent visible light degradation activity for methylene blue," *Applied Surface Science*, vol. 396, pp. 58–66, 2017.